

Dynamic sampling and information encoding in biochemical networks

Garrett D. Potter,¹ Tommy A. Byrd,² Andrew Mugler,² and Bo Sun¹

¹*Department of Physics, Oregon State University, Corvallis, OR USA*

²*Department of Physics and Astronomy, Purdue University, West Lafayette IN, USA*

Cells use biochemical networks to translate environmental information into intracellular responses. These responses can be highly dynamic, but how the information is encoded in these dynamics remains poorly understood. Here we investigate the dynamic encoding of information in the ATP-induced calcium responses of fibroblast cells, using a vectorial, or multi-time-point, measure from information theory. We find that the amount of extracted information depends on physiological constraints such as the sampling rate and memory capacity of the downstream network, and is affected differentially by intrinsic vs. extrinsic noise. By comparing to a minimal physical model, we find, surprisingly, that the information is often insensitive to the detailed structure of the underlying dynamics, and instead the decoding mechanism acts as a simple low-pass filter. These results demonstrate the mechanisms and limitations of dynamic information storage in cells.

Cells utilize cascades of biochemical pathways in order to translate environmental cues into intracellular responses [1, 2]. Due to extensive feedbacks and cross-talk among these signaling pathways [3–6], messenger molecules exhibit rich dynamic modes, such as waves, oscillations, and pulses. Recent work in cell biology has suggested a new perspective in cell signaling: the dynamics, or temporal profiles, of messenger molecules allow cells to encode and decode even more rich and complex information than static profiles do [7, 8]. For instance, during inflammation response, exposure to tumor necrosis factor- α (TNF α) causes the transcription factor NF- κ B to oscillate between the nucleus and cytoplasm of a cell [9], whereas bacterial lipopolysaccharide (LPS) triggers a single wave of NF- κ B within the cell [10]. Therefore, the dynamics of NF- κ B encode the identity of external stimuli. In another example, stimulation of pheochromocytoma cells (PC12) cells by epidermal growth factor (EGF) leads to transient mitogen-activated protein kinase (MAPK) activation and cell proliferation, whereas stimulation by nerve growth factor (NGF) leads to sustained MAPK activation and cell differentiation [11]. These and other examples raise the question of how one quantifies the information carried by signaling dynamics.

Information theory provides a useful framework to address such questions [12–14]. In the simplest case, one calculates the scalar mutual information between states of extracellular stimuli (typically well-controlled discretized values) and states of the cell (typically protein concentrations measured at a certain time). Mutual information characterizes the correlation between environmental cues and cell responses, and conveniently expresses such correlations in units of bits. This unified framework has been successfully employed to quantitatively understand the amount of information that can be transmitted through a biochemical pathway (channel capacity) [15], mechanisms of mitigating errors [16], and design principles of signaling network architectures [17].

Recently, inspired by the fact that cells utilize dynamic

signaling to encode and decode information, a multivariate, or vectorial, mutual information has been proposed [18]. In this new framework, cellular responses are described by vectors of dimension n , which consist of cellular states sampled at multiple time points. The vectorial mutual information is generally higher than the scalar mutual information, indicating that signaling dynamics indeed allow richer content to be transmitted. It has also been shown that sampling cellular states at multiple time points eliminates extrinsic noise—noise that degrades information due to cell-to-cell variability.

In light of these results, we ask what is the optimal strategy for cells to utilize the power of vectorial mutual information? How should a cell sample its own temporal profiles? Can cells use vectorial mutual information to distinguish different dynamic states of the underlying signaling pathways? To address these questions, we combine experimental measurements of ATP-induced Ca²⁺ responses with theoretical analysis, to systematically study scalar and vectorial mutual information in a dynamic signaling system. We find that given different physiological constraints, the optimal sampling depends on the starting time, sampling rate and memory capacity. We characterize how vectorial information is affected by intrinsic and extrinsic noise, in both the experimental system and a simple physical model. Surprisingly, we find that vectorial mutual information is often insensitive to the detailed structure of the underlying dynamics, failing to distinguish between, for example, oscillatory and relaxation dynamics. We explain this observation by deriving the connections between vectorial and scalar information, which reveals that in a particular regime vectorial encoding acts as a simple low-pass filter.

RESULTS

To investigate properties of dynamic encoding, we focus on the calcium dynamics of fibroblast cells in response to extracellular adenosine triphosphate (ATP), a com-

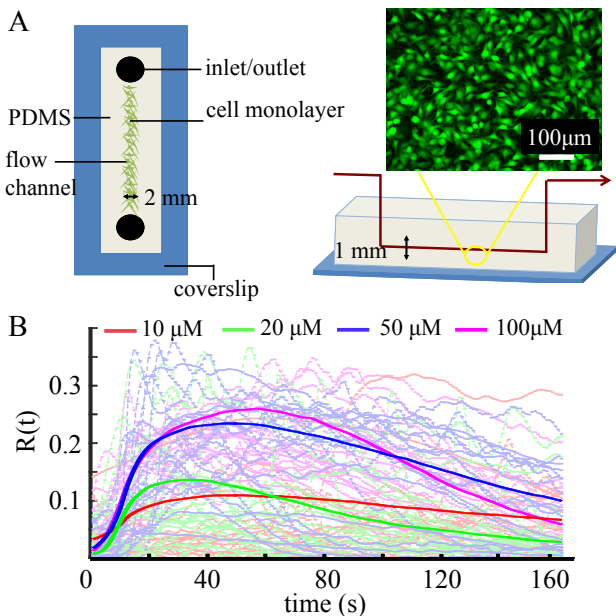


FIG. 1. Schematics of experimental setup. (A) The top and cross view of the microfluidic device to deliver ATP solution to cultured fibroblast (NIH 3T3) cells. Inset: fluorescent calcium imaging of a typical experiment. (B) Relative fluorescent intensities indicating the calcium dynamics $R_i(t)$ of individual cells (dashed lines) and their average (solid lines) when stimulated by external ATP at four different concentrations.

mon signaling molecule involved in a range of physiological processes such as platelet aggregation [19] and vascular tone [20]. ATP is detected by P2 receptors on the cell membrane, and triggers the release of second messenger inositol trisphosphate (IP3). IP3 activates the ion channels on endoplasmic reticulum (ER) which allows free calcium ions to flux into the cytosol. The nonlinear interactions of Ca^{2+} , IP3, ion channels and ion pumps generate various types of calcium dynamics which may lead to distinct cellular functions [8, 21].

Quantifying information in experimental dynamics

In order to measure the calcium dynamics of fibroblast cells in response to external ATP stimuli, we employ microfluidic devices for cell culture and solution delivery as described previously [22, 23]. In brief, NIH 3T3 cells (ATCC) are cultured in the PDMS (Polydimethylsiloxane) bounded flow channels as shown in Fig. 1A. A small fraction of red-fluorescent labeled MDA-MB-231 cells have also been cocultured with fibroblast cells as a viability control, and are not included in subsequent analysis. After attaching the glass bottom for 24 hours, the cells are loaded with fluorescent calcium indicators (FLUO-4, Thermo Fisher Scientific) according to the manufacturer's protocol. ATP solutions diluted by

DMEM (Dulbecco's Modified Eagle Medium) into 10, 20, 50, and 100 μM are sucked into the flow channel with a two-way syringe pump (New Era Pump Systems Inc.) at a rate of 90 $\mu\text{L}/\text{min}$. At the same time, we record fluorescent images of the cell monolayer at 4 Hz for a total of 10 minutes (Hamamatsu Flash 2.8).

In all the experimental recordings, ATP arrives at approximately $t = 10$ sec, and stays at a constant concentration. Since most responses happen within 2 minutes, we use the first 160 seconds of recording for subsequent analysis. The time-lapse images are post-processed to obtain the fluorescent intensity $I_i(t)$ of each cell i at a given time t . We define the calcium response as $R_i(t) = [I_i(t) - I_i^r]/I_i^r$, where I_i^r is a reference obtained by averaging the fluorescent intensity of cell i before ATP arrives (Fig. 1B).

In order to quantify the information encoded in the calcium dynamics of fibroblast cells in response to ATP, we have analyzed a total of more than 10,000 cells over 4 different ATP concentrations (10, 20, 50, 100 μM) as inputs. With the underlying assumption that each input appears at probability of 1/4, the same number of cells are selected for each ATP concentration. The maximum possible mutual information between the input and output is therefore $\log_2 4 = 2$ bits.

Denoting the dynamic calcium response as $R_i^\alpha(t)$, where $\alpha = 1, 2, 3, 4$ for each ATP concentration, and $i = 1, 2, \dots, N$ for each cell ($N \sim 2,500$), the scalar mutual information is defined as

$$MI_s(t) = H[\{R(t)\}] - \frac{1}{4} \sum_{\alpha} H[\{R^\alpha(t)\}], \quad (1)$$

where H represents the differential entropy, which we calculate using the k-nearest neighbor method [18, 24]. The first term is the unconditioned entropy calculated from cellular responses at time t of all four ATP concentrations. The second term is the average of differential entropy conditioned at each ATP concentration. The scalar mutual information $MI_s(t)$ measures how much the entropy in the output (cellular responses) is reduced by knowledge of the input (ATP concentration). It is a function of the time t at which we take a snapshot of the system and evaluate the differential entropy across the ensemble of cells.

The vectorial mutual information is defined as

$$MI_v(t_s) = H[\{\vec{R}(\vec{t})\}] - \frac{1}{4} \sum_{\alpha} H[\{\vec{R}^\alpha(\vec{t})\}], \quad (2)$$

where $\vec{t} = (t_s, t_s + r^{-1}, t_s + 2r^{-1}, \dots, t_s + T_d)$. When generalizing to the vectorial mutual information MI_v , one has to specify not only the sampling start time t_s (equivalent to the time t in the case of MI_s), but also the sampling duration T_d and the sampling rate r , which opens the possibility of complex sampling strategies. In the time between t_s and $t_s + T_d$, a fibroblast cell sampling its calcium concentration at a rate r accumulates

a vectorial representation of its calcium dynamics with vector dimension $n = 1 + rT_d$. Since the cell has to store the vector for further processing, n also represents its memory capacity.

Dynamic encoding increases information

We first consider the situation where the sampling duration T_d is fixed. Fig. 2 shows the mutual information of both scalar (MI_s) and vectorial encoding (MI_v) from fibroblast calcium dynamics for $T_d = 30$ sec (A, C, E) and $T_d = 60$ sec (B, D, F). As seen in Fig. 2A and B, MI_s first rises, then falls, as a function of time. This is due to the separation, then convergence, of the four ATP-conditioned responses as a function of time, as seen in Fig. 1B: better-separated responses contain more information about the ATP level. This shape is also reflected in MI_v , with additional smoothing due to the repeated sampling.

Fig. 2A and B also show that MI_v increases with sampling rate r . This is intuitive, since a larger sampling rate produces a larger number of samples $n = 1 + rT_d$, which increases the amount of information extracted from the dynamics. While the results in Fig. 2A and B are intuitively expected, it is also important to know the efficiency for dynamic encoding. To this end, we have calculated the mutual information per sample, defined as MI_v/n , as shown in Fig. 2C and D. It is evident that higher coding efficiency is achieved at smaller sampling rate. This is because when the sampling rate is large, samples are spaced closely in time, and therefore contain increasingly redundant information, which lowers the coding efficiency. The results shown in Fig. 2C and D suggest that although dynamic encoding mitigates intrinsic noise, it is not enough to allow MI_v to grow faster than linearly with n . Indeed, scalar encoding generally offers better efficiency than vectorial encoding: as shown in both Fig. 2C and D, $MI_s(t_s) > MI_v(t_s)/n$, except at very early times when the cellular response has just started.

The results of Fig. 2A-D are summarized in Fig. 2E and F, which plot MI_{max} , the maximum mutual information over all possible sampling start times t_s . As seen in Fig. 2E and F, MI_{max} monotonically increases with n , which shows that dynamic encoding improves the information capture. However, the increase is sublinear, i.e. below the dashed line defined by the scalar mutual information, which shows that the efficiency of dynamic encoding decreases with vector length n . Considering scalar encoding as the limiting case of $r \rightarrow 0$, we conclude that as the sampling rate increases, mutual information increases but the coding efficiency per measurement decreases.

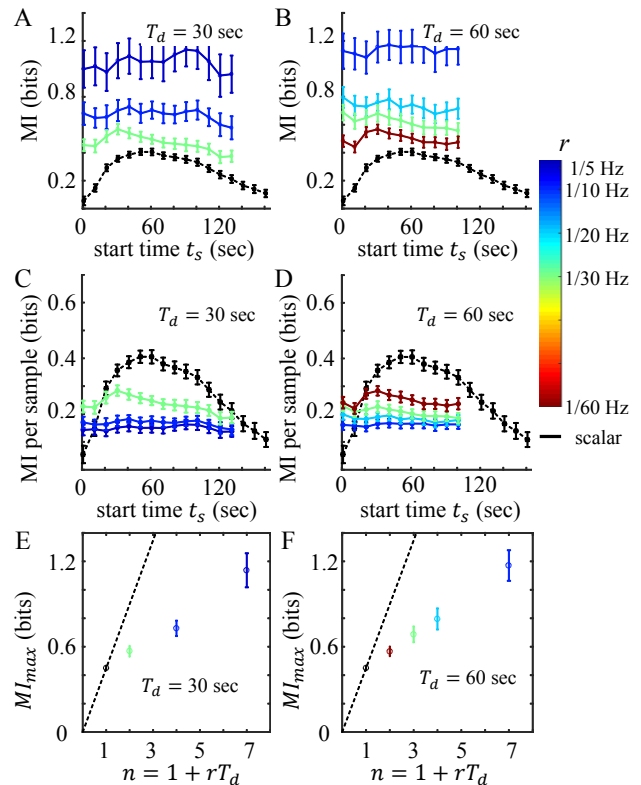


FIG. 2. Information carried by calcium dynamics of fibroblast cells in response to ATP, for fixed sampling duration T_d . (A, B) Vectorial mutual information MI_v as a function of sampling start time t_s at different sampling rates r (color bar), for (A) $T_d = 30$ sec and (B) $T_d = 60$ sec. Black curve is scalar mutual information MI_s at each time point. (C, D) Mutual information per sample for the same conditions as A, B. (E, F) Maximum MI_v over all t_s values, as a function of the memory capacity n , for (E) $T_d = 30$ sec and (F) $T_d = 60$ sec. Maximum MI_s is plotted at $n = 1$. Error bars in A-F represent the means and standard deviations of 100 bootstraps.

Dynamics determine optimal sampling rate

Cells have limited ability to process dynamically encoded information. It is conceivable that a biochemical signaling network processing a vectorial code of high dimension will be complex and expensive, because it requires a high memory capacity n for storage and transfer. Therefore a relevant question is, what sampling strategy can a cell apply when the memory capacity is fixed? Fig. 3A and B show the mutual information as a function of sampling start time t_s when the memory capacity n is fixed, while the sampling rate r , and therefore the duration $T_d = (n - 1)/r$, are allowed to vary. Comparing Fig. 3A to B, we see that larger memory capacity n generally allows more information to be transmitted, as was the case in Fig. 2. This trend is quantified in Fig. 3C, which plots the mutual information as a function of n , for fixed sampling rate and at two particular starting times t_s . We

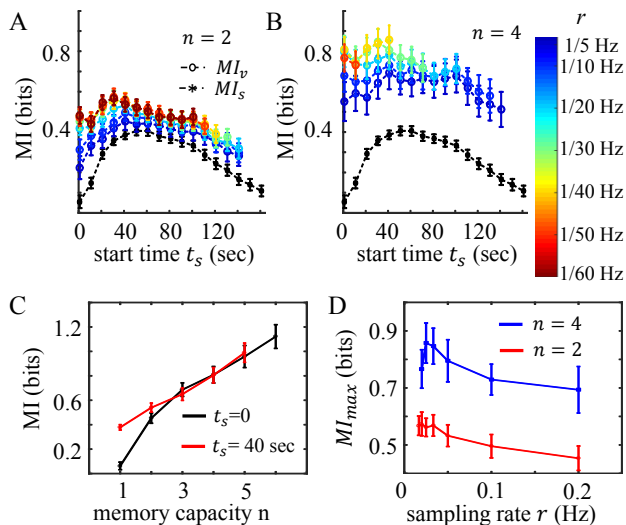


FIG. 3. Information carried by calcium dynamics of fibroblast cells in response to ATP, for a given memory capacity n . (A, B) Vectorial mutual information MI_v as a function of sampling start time t_s at different sampling rates r (color bar) for (A) $n = 2$ and (B) $n = 4$. Black curve is scalar mutual information MI_s each time point. (C) MI_v as a function of n at fixed sampling rate $r = 1/30$ Hz and sampling start time (black curve $t_s = 0$, red curve $t_s = 40$ sec). $n = 1$ corresponds to MI_s . (D) Maximum MI_v over all t_s values, as a function of r , for fixed memory capacity (red $n = 2$, blue $n = 4$). Error bars in A-D represent the means and standard deviations of 100 bootstraps.

see that the amount of information significantly depends on t_s for small n , while the difference diminishes at larger n . This is because information is upper-bounded (at 2 bits in our case), which requires that all curves, regardless of t_s , ultimately saturate with increasing n . Therefore we see that larger memory capacity not only encodes higher information, but also helps cells to obtain more uniform readouts.

We also see in Fig. 3A and B that for a given n , there is an optimal sampling rate r that maximizes the information. This is made more evident by considering, as before, the maximum mutual information MI_{max} over all possible start time t_s , which is plotted as a function of r in Fig. 3D. Particularly, for $n = 4$ (blue curve), we see that MI_{max} is maximal at a particular sampling rate. This is because, for a fixed number of samples n , sampling too frequently results in redundant information, as discussed above; while sampling too infrequently places samples at late times, when the dynamic responses have already relaxed (see Fig. 1B). Therefore it is generally beneficial to sample at a lower rate except when the sampled points are too far apart, which places samples outside the ‘high yield’ temporal region. The tradeoff between these two effects leads to the optimal sampling rate, where the information gathered is the largest.

Vectorial information is insensitive to detailed dynamic structure

Is vectorial encoding sensitive to the underlying details of the dynamic response? In order to answer this question, and to provide a mechanistic understanding of dynamic information transmission in biochemical networks, we construct a minimal stochastic model with the aim of recapitulating the key features of the fibroblast response. As a minimal model we consider a damped harmonic oscillator in a thermal bath, driven out of equilibrium by a time-dependent forcing $F(t)$. The magnitude of the external forcing is proportional to a scalar input, which is analogous to the ATP concentration. The displacement of the particle $x(t)$, like the calcium dynamics, can then be analyzed to infer the information that the oscillator encodes about the input.

The equation of motion for the oscillator is given by the Langevin equation [25]

$$m \frac{d^2 x}{dt^2} + \gamma \frac{dx}{dt} + kx = g_\alpha F(t) + \psi(t),$$

$$\langle \psi(t) \psi(t') \rangle = 2k_B T \gamma \delta(t - t'),$$

$$F(t) = \begin{cases} 0 & t < t_1 \\ 1 & t_1 \leq t \leq t_2 \\ e^{-\beta(t-t_2)} & t > t_2. \end{cases} \quad (3)$$

Here m is the mass, γ is the drag coefficient, and k is the spring constant. $\psi(t)$ is the random forcing arising from thermal fluctuations with energy $k_B T$; it is Gaussian and white, and represents intrinsic noise. The form of the external forcing $F(t)$, illustrated in Fig. 4A for four magnitudes $g_{1,2,3,4}$, is chosen to reflect the fact that following initial elevation, cells relax to their resting level of cytosolic calcium concentration at the end of experimental recording (see Fig. 1B). To account for the extrinsic noise observed in our cellular system [26], we have allowed the spring constant for each oscillator trajectory to vary uniformly around $\langle k \rangle$ with a standard deviation δk . Fig. 4B shows sample trajectories $x(t)$ for two cases: when the oscillations are overdamped ($m < m_c$) or underdamped ($m > m_c$), where $m_c \equiv \gamma^2/(4k)$ is the mass at critical damping.

Fig. 4C and D show, for the overdamped and underdamped cases, the scalar and vectorial mutual information between input g_α and output $x(t)$, as a function of sampling start time t_s , for various sampling rates r and fixed memory capacity $n = 2$. Additionally, Fig. 4E shows the mutual information as a function of n at fixed r for the overdamped case, while Fig. 4F shows the maximum mutual information as a function of r at fixed n for both cases. Comparing Fig. 4 to Fig. 3, we see that our minimal model is sufficient to capture the key features of the experiments. Specifically, comparing Fig. 4C and D to Fig. 3A, we see that the model captures the non-monotonic shape of the mutual information as a function

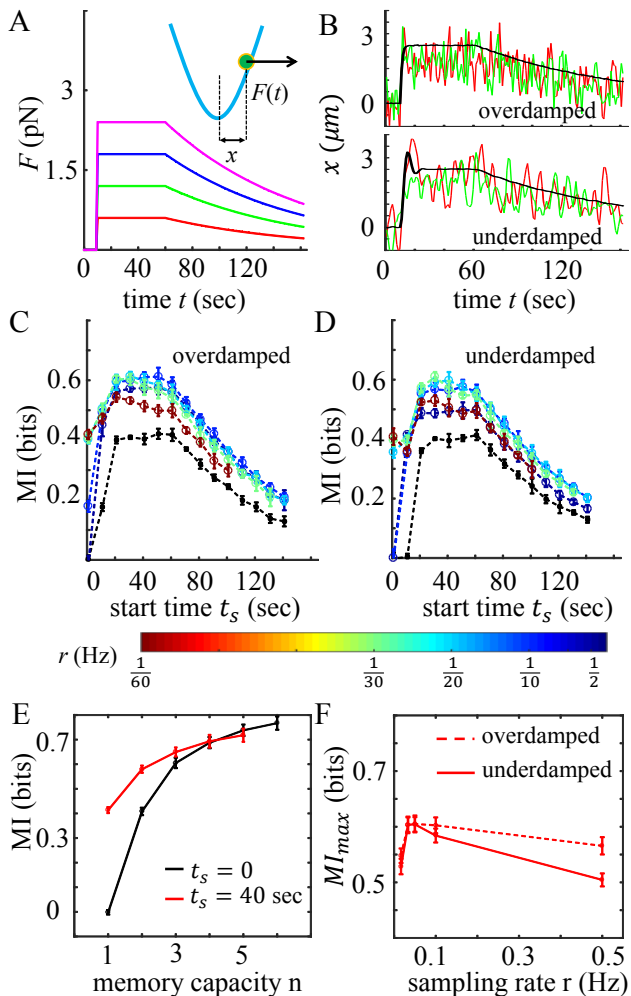


FIG. 4. Information encoding in the noisy harmonic oscillator model. (A) Oscillator at position $x(t)$ is subjected to random thermal forcing as well as deterministic forcing $F(t)$ (Eq. 3). Four force magnitudes $g_{1,2,3,4} = \{0.6 \text{ pN}, 1.2 \text{ pN}, 1.8 \text{ pN}, 2.4 \text{ pN}\}$ serve as input, while $x(t)$ is output. Other parameters are $t_1 = 10 \text{ sec}$, $t_2 = 60 \text{ sec}$, and $\beta = 0.01 \text{ sec}^{-1}$. (B) Two sample trajectories (red and green curves) and the average of 5,000 trajectories (black curves) corresponding to $g_4 = 2.4 \text{ pN}$. Upper: overdamped oscillators with $m = 0.4m_c$, where $m_c = \gamma^2/(4k) = 0.25 \text{ mg}$ is the mass at critical damping, $\gamma = 1 \text{ pN}\cdot\text{sec}/\mu\text{m}$, and $k = 1 \text{ pN}/\mu\text{m}$. Lower: underdamped oscillators with $m = 9m_c$. Other parameters are $k_B T = 0.5 \text{ pN}\cdot\mu\text{m}$ and $\delta k = 0.2 \text{ pN}/\mu\text{m}$. (C, D) Vectorial mutual information MI_v as a function of sampling start time t_s at different sampling rates r (color bar) and memory capacity $n = 2$, for (C) overdamped and (D) underdamped oscillators. Black curve is scalar mutual information MI_s each time point. (E) MI_v as a function of n at fixed sampling rate $r = 1/30 \text{ Hz}$ and sampling start time (black curve $t_s = 0$, red curve $t_s = 40 \text{ sec}$). $n=1$ corresponds to MI_s . (F) Maximum MI_v over all t_s values, as a function of r , for fixed memory capacity $n = 2$. Error bars in C-F represent the means and standard deviations of 20 independent trials each.

of start time t_s , as well as the improvement of vectorial encoding (colors) over scalar encoding (black). Comparing Fig. 4E to Fig. 3C, we see that the model captures the increase of mutual information with memory capacity n , as well as the large- n convergence of curves with different t_s . Finally, comparing Fig. 4F to Fig. 3D, we see that the model captures the presence of an optimal sampling rate r that negotiates the tradeoff between samples that are well-separated, yet confined to the high-yield region ($t_1 \leq t \leq t_2$ in the model). These correspondences validate the model, and allow us to use the model to ask how vectorial encoding depends on the structure of the underlying dynamic responses.

The noisy oscillator model allows us to explore two qualitatively different regimes of dynamic structure. In the overdamped regime, the thermal noise overpowers the oscillations, and the dynamics are dominated by fluctuations (Fig. 4B, upper). In contrast, in the underdamped regime, the oscillations overpower the thermal noise, and the dynamics are dominated by the underlying oscillatory structure (Fig. 4B, lower). Since vectorial mutual information corresponds to sampling the dynamics at regular intervals, it is natural to hypothesize that the amount of information extracted from underdamped dynamics will be higher than that extracted from overdamped dynamics, because underdamped dynamics have a more ordered structure. Fig. 4C and D compare the mutual information in the overdamped and underdamped cases. Surprisingly, we see that the amounts of information are roughly equivalent in the two cases. It is evident from Fig. 4C and D that the equivalence holds at varying sampling rates r and start times t_s (including the start time at which the information is maximal, Fig. 4F). In particular, the equivalence holds when the sampling rate r equals the oscillation frequency of the underdamped oscillator, $\nu = \sqrt{(k/m)(1 - m_c/m)}/(2\pi) \approx 1/10 \text{ Hz}$ in Fig. 4. This is true despite the fact that $r = \nu$ is where we would have expected the vectorial information to benefit most from sampling the periodic dynamics instead of noisy dynamics. We have also checked that the equivalence holds for a large range of intrinsic and extrinsic noise levels. The previously demonstrated correspondence between the model and the experiments suggests that in the fibroblasts as well, ordered dynamics would not provide more information than noisy dynamics, at least as quantified by the vectorial mutual information. We expand upon this conclusion in the Discussion.

Differential effects of intrinsic and extrinsic noise

Vectorial mutual information MI_v is larger than scalar mutual information MI_s in part because repeated sampling helps to mitigate intrinsic noise [18]. Yet, in the case of the fibroblast cells, the gain of MI_v over MI_s is often small. For example, as seen in Fig. 3A, at $n = 2$ and

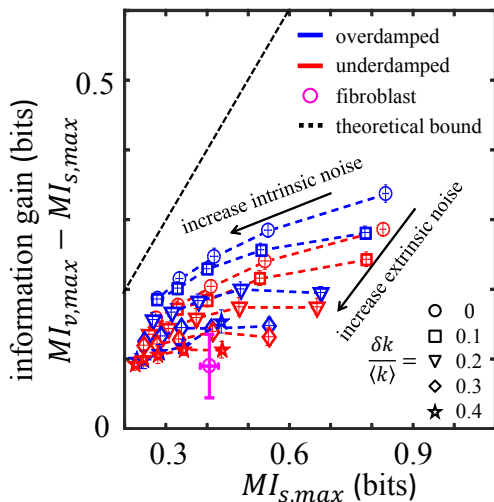


FIG. 5. Gain of vectorial over scalar mutual information, where each is maximized over start times t_s . For vectorial information, memory capacity is $n = 2$ and sampling rate is $r = 1/10$ Hz. Fibroblast data are compared against over- and underdamped oscillator models and detailed model of calcium dynamics [26]. In oscillator model, parameters are as in Fig. 4, and intrinsic noise is governed by $k_B T$, which varies from 0.2 to 1 pN $\cdot\mu\text{m}$, while extrinsic noise is governed by $\delta k / \langle k \rangle$, which varies from 0 to 0.4. In calcium model, extrinsic noise is governed by parameter fold-change factor F [26]. Error bars represent means and standard deviations of 100 bootstraps (fibroblast data), 20 independent trials of 5,000 trajectories each (oscillator model).

$r = 1/10$ Hz, whereas MI_s can be as large as ~ 0.4 bits, the further increase of MI_v over MI_s is less than ~ 0.1 bits. We make this observation quantitative by defining the information gain $MI_{v,max} - MI_{s,max}$, where each is maximized over the start time t_s . Fig. 5 shows the information gain vs. $MI_{s,max}$ for the fibroblasts at $n = 2$ and $r = 1/10$ Hz (pink circle). The fact that the gain is small (0.1 bits) suggests that additional factors, apart from intrinsic noise alone, reduce the efficacy of vectorial encoding.

To explore this hypothesis in a systematic way, we again turn to our minimal oscillator model. For both the overdamped and underdamped oscillator, we compute $MI_{s,max}$ and the information gain. In the model, the intrinsic noise is governed by the thermal energy $k_B T$. The model also provides an opportunity to investigate the effects of extrinsic noise, which is governed by $\delta k / \langle k \rangle$, the relative width of the distribution of spring constants. As shown in Fig. 5, when the intrinsic noise increases while the extrinsic noise is fixed, both the scalar information and the information gain decrease, as expected (dashed lines). The decrease in scalar information is more pronounced than the decrease in the gain, which is consistent with the fact that vector information is beneficial for mitigating intrinsic noise. On the other hand, when the extrinsic noise increases while the intrinsic noise is fixed,

the gain decreases more rapidly, while the scalar information decreases less rapidly (the different symbols). This implies that the gain is more sensitive to extrinsic noise than intrinsic noise.

In the context of the fibroblast population, these results suggest that extrinsic noise (cell-to-cell variability), not intrinsic noise, is primarily responsible for degrading the performance of vectorial encoding and producing small information gains.

Redundant information and low-pass filtering

The vectorial mutual information MI_v can never be larger than the sum of the scalar mutual information values $MI_s(t_i)$ taken individually at each time point t_i . The reason is that there will always be some nonnegative amount of redundant information between the output at one time and the output at another time. Denoting the redundant information as MI_{red} , we formalize this statement as

$$MI_{red} = \left[\sum_{i=1}^n MI_s(t_i) \right] - MI_v = n \langle MI_s \rangle - MI_v \geq 0, \quad (4)$$

where as before $t_i = t_s + ir^{-1}$, and in the second step we rewrite the sum in terms of the temporal average $\langle MI_s \rangle = n^{-1} \sum_{i=1}^n MI_s(t_i)$. In the limit that the dynamics are approximately stationary, such as in the high-yield regions of Figs. 1B and 4B, MI_s is approximately independent of time, and $\langle MI_s \rangle = MI_s$. For $n = 2$, as in Fig. 5, Eq. 4 then becomes

$$MI_v - MI_s \leq MI_s. \quad (5)$$

Eq. 5 expresses the intuitive fact that the gain upon making an additional measurement can never be more than the information from the original measurement, for a stationary process. Eq. 5 is plotted in Fig. 5 (dash-dotted line), and we see that it indeed bounds all data from above, as predicted.

The redundant information in Eq. 4 can be directly measured in the experiments. Fig. 6A shows the redundant information in the fibroblast calcium dynamics as a function of the memory capacity n , computed from the scalar and vectorial mutual information according to Eq. 4. We see that the redundant information depends on the sampling rate r (symbols) and appears to be bounded from above by a roughly linear function of n . Can we understand this dependence theoretically? To address this question, we return to Eq. 4. We rearrange Eq. 4 as $MI_{red} = (n - 1) \langle MI_s \rangle - \Delta$, where we define $\Delta = MI_v - \langle MI_s \rangle$. Since the vectorial information is not smaller than the scalar information corresponding to any of its time points, it is also not smaller than the average scalar information. Therefore, $\Delta \geq 0$, and we have

$$MI_{red} \leq (n - 1) \langle MI_s \rangle \quad (6)$$

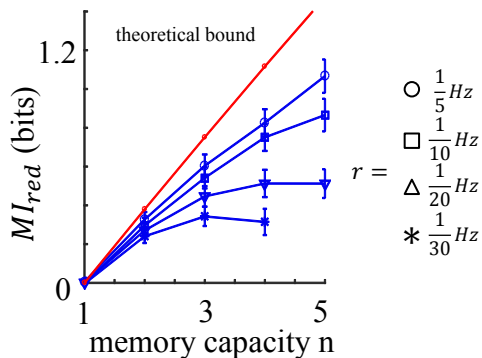


FIG. 6. Redundant information of dynamic encoding for fibroblast cells. Redundant information MI_{red} (Eq. 4) is plotted as a function of memory capacity n for varying sampling rates r and compared with the theoretical bound (Eq. 6).

Eq. 6 is a linear function of n , weakly modified by the fact that $\langle MI_s \rangle$ itself depends on n since it is computed for varying numbers of time points. Eq. 6 is compared with the data in Fig. 6, and we see that it indeed predicts the bound well. Eq. 6 makes another prediction, namely that the bound is reached for a stationary process when $\Delta = MI_v - \langle MI_s \rangle \rightarrow 0$, i.e. when the vector information provides vanishing improvement over the average scalar information. We expect this situation to occur in the limit of large sampling frequency r , when samples occur in close succession and offer little additional information beyond a single, scalar measurement. Indeed, we see from the data in Fig. 6 that consistent with this prediction, the bound is approached in the limit of increasing r .

Clearly, the benefit of vectorial encoding is largest when the redundant information is small (the lowest data points in Fig. 6). In the ideal case, there is no redundant information at all, and Eq. 4 becomes

$$MI_v = \sum_{i=1}^n MI_s(t_i). \quad (7)$$

Here, we see that the vectorial information is simply the sum of the scalar information at each time point. In this sense, Eq. 7 describes a low-pass filter: vectorial encoding captures the temporal accumulation of scalar information, as long as the sampling is sufficiently slow to remove the redundancy. Therefore, in this limit the vectorial information records only the slow (low-frequency) variations in the dynamics. This feature may help explain the previous counterintuitive result that the vectorial information is insensitive to the detailed dynamic structure, as we expand upon in the Discussion.

DISCUSSION

The dynamic waveforms of signaling molecules have offered a new perspective to understand cellular infor-

mation encoding. Indeed, dynamic encoding, as quantified by the vectorial mutual information MI_v , has larger channel capacity than the static encoding, as quantified by the scalar mutual information MI_s [18]. From both experimental data and a minimal model we presented here, we find that dynamic encoding has several key advantages over static encoding. First, the maximal vectorial information is larger than the maximal scalar information, suggesting that dynamic encoding provides a more reliable readout of environmental inputs than static encoding does. Second, while the scalar information can vary significantly with sampling time, the vectorial information is more uniform across sampling start times, even with small vector dimensions (Fig. 3C and Fig. 4E).

However, the benefit of dynamic encoding comes with the cost of increasing the memory capacity n of cells. For a fixed memory capacity, we have shown that the best strategy for cells to adopt is to sample as slowly as possible while keeping their samples within a “high-yield” region, where the mean dynamics depend significantly on the input. Nonetheless, we find that within this region, the benefit of dynamic encoding can depend very little on the detailed structure of the dynamics (persistent oscillation vs. monotonic relaxation). Moreover, the gain of dynamic encoding over static encoding can be small, largely due to the presence of extrinsic, as opposed to intrinsic, noise.

The finding that vectorial information is largely insensitive to the detailed dynamics is surprising, and is likely a reflection of the type of dynamics we investigate here, as well as the vectorial measure itself. To accurately model the experimental dynamics, we have considered noisy dynamics arising from a driven oscillator. Although this has allowed us to probe both noise-dominated and oscillation-dominated regimes, these dynamics remain mean-reverting and confined to a stationary or cyclo-stationary state. It is likely that other classes of dynamics, such as temporal ramps, would emerge as having uniquely higher vectorial information than stationary dynamics. Furthermore, the vectorial information itself, as defined here, reports correlations between a categorical input variable and a regularly sampled output trajectory. It is likely that more sophisticated information-theoretic measures would be more sensitive to dynamic details, such as the mutual information between input and output trajectories, which has been argued to play a biological role in cell motility [27, 28].

Our results suggest that dynamic and static encoding mechanisms are deeply connected. By introducing the redundant information MI_{red} , we have made this connection rigorous. Specifically, combining Eqs. 4 and 6 yields $\langle MI_s \rangle \leq MI_v \leq n \langle MI_s \rangle$, which shows explicitly that the vectorial information is bounded from both above and below by quantities determined by the window-averaged scalar information $\langle MI_s \rangle$. Taking a window average of the scalar information is equivalent to the downstream

network acting as a low-pass filter, accumulating temporal measurements at sufficiently low frequencies. We find that such low-pass filtering effects are evident from both the experimental and modeling results.

In this study we have taken the approach that an understanding of both the static and dynamic encoding behaviors of the fibroblast cells can be obtained from a model based on noisy harmonic oscillators. Despite the simplicity of the model, we find that it reproduces the experimental results very well. The agreement between the experiment and this simple model highlights our central conclusion: the vectorial mutual information is intrinsically connected with the scalar mutual information and therefore has limited capability to distinguish underlying dynamics. Because the model is minimal, we anticipate that it can be extended to answer more general questions about information encoding on a large, multicellular scale. This is particularly desirable as understanding collective information processing is a new frontier in systems biophysics [22, 23, 26, 29–31].

-
- [1] A. Pires-daSilva and R. J. Sommer, *Nature Reviews Genetics* **4**, 39 (2003).
- [2] R. P. Bhattacharyya, A. Reményi, B. J. Yeh, and W. A. Lim, *Annu Rev. Biochem.* **75**, 655 (2006).
- [3] J. A. Papin, T. Hunter, B. O. Palsson, and S. Subramaniam, *Nature Reviews Molecular Cell Biology* **6**, 99 (2005).
- [4] W. Lim, B. Mayer, and T. Pawson, *Cell Signaling* (Garland Science, 2014).
- [5] J. R. Mestre, P. J. Mackrell, D. E. Rivadeneira, P. P. Stapleton, T. Tandabe, and J. M. Daly, *J. Biol. Chem.* **276**, 3977 (2001).
- [6] J. S. Logue and D. K. Morrison, *Genes and Dev.* **26**, 641 (2012).
- [7] B. N. Kholodenko, *Nat. Rev. Mol. Cell Biol.* **7**, 165 (2006).
- [8] J. E. Purvis and G. Lahav, *Cell* **152**, 945 (2013).
- [9] A. Hoffmann, A. Levchenko, M. L. Scott, and D. Baltimore, *Science* **298**, 1241 (2002).
- [10] M. W. Covert, T. H. Leung, J. E. Gaston, and D. Baltimore, *Science* **309**, 1854 (2005).
- [11] C. J. Marshall, *Cell* **80**, 179 (1995).
- [12] C. Adami, *Physics of Life Reviews* **1**, 3 (2004).
- [13] W. Bialek, *Biophysics: Searching for Principles* (Princeton University Press, 2012).
- [14] A. Levchenko and I. Nemenman, *Current Opinion in Biotechnology* **28**, 156 (2014).
- [15] R. Cheong, A. Rhee, C. J. Wang, I. Nemenman, and A. Levchenko, *Science* **334**, 354 (2011).
- [16] S. Uda, T. H. Saito, T. Kudo, T. Kokaji, T. Tsuchiya, H. Kubota, Y. Komori, Y. Ozaki, and S. Kuroda, *Science* **341**, 558 (2013).
- [17] M. Voliotis, R. M. Perrett, C. McWilliams, C. A. McArdle, and C. G. Bowsher, *Proc. Nat. Acad. Sci.* **111**, E326 (2014).
- [18] J. Selimkhanov, B. Taylor, J. Yao, A. Pilko, J. Albeck, A. Hoffmann, L. Tsimring, and R. Wollman, *Science* **346**, 1370 (2014).
- [19] C. Léon, B. Hechler, M. Freund, A. Eckly, C. Vial, P. Ohlmann, A. Dierich, M. LeMeur, J. Cazenave, and C. Gachet, *J. Clin. Invest.* **104**, 1731 (1999).
- [20] S. Yitzhaki, A. Shainberg, Y. Cheporko, B. A. Vidne, A. Sagie, K. A. Jacobson, and E. Hochhauser, *Biochemical Pharmacology* **72**, 949 (2006).
- [21] M. Falcke, *Advances in Physics* **53**, 255 (2004).
- [22] B. Sun, J. Lembong, V. Normand, M. Rogers, and H. A. Stone, *Proc. Nat. Aca. Sci* **109**, 7759 (2012).
- [23] B. Sun, G. Doclos, and H. A. Stone, *Phys. Rev. Lett.* **110**, 158103 (2013).
- [24] D. O. Loftsgaarden and C. P. Quesenberry, *Ann. Math. Statist* **36**, 1049 (1965).
- [25] N. G. V. Kampen, *Stochastic Processes in Physics and Chemistry* (Elsevier, 2007).
- [26] G. D. Potter, T. A. Byrd, A. Mugler, and B. Sun, arXiv preprint arXiv:1508.06966 (2015).
- [27] F. Tostevin and P. R. Ten Wolde, *Physical review letters* **102**, 218101 (2009).
- [28] F. Tostevin and P. R. Ten Wolde, *Physical Review E* **81**, 061917 (2010).
- [29] A. Mugler, A. Levchenko, and I. Nemenman, *Proceedings of the National Academy of Sciences*, 201509597 (2016).
- [30] D. Ellison, A. Mugler, M. D. Brennan, S. H. Lee, R. J. Huebner, E. R. Shamir, L. A. Woo, J. Kim, P. Amar, I. Nemenman, *et al.*, *Proceedings of the National Academy of Sciences*, 201516503 (2016).
- [31] B. A. Camley, J. Zimmermann, H. Levine, and W.-J. Rappel, arXiv preprint arXiv:1506.06698 (2015).